JEE Journal of Ecological Engineering

Journal of Ecological Engineering, 2026, 27(9), 264–279
https://doi.org/10.12911/22998993/221855
ISSN 2299–8993, License CC-BY 4.0

Received: 2026.04.21
Accepted: 2026.07.15
Published: 2026.08.01

Parametric evaluation of orifice plate-based hydrodynamic cavitation for tartrazine removal: A Taguchi L9 approach

Segundo Alberto Vásquez Llanos[1*], Sebastian Huangal Scheineder[1], Marilín Sánchez Purihuaman[2], Magali Camila Vivas-Cuellar[3], Karina Del Pilar Rivadeneira Sipion[4], Carmen Carreño-Farfán[2], Esteban C. Castellanos Borrero[5], Juan Taumaturgo Medina Collana[6], Ada Patricia Barturen Quispe[1]

[1] Centro de Investigación Medio Ambiente y Desarrollo Sostenible, Facultad de Ingeniería Química e Industrias Alimentarias, Universidad Nacional Pedro Ruiz Gallo, Perú
[2] Grupo de investigación BlyME:BS-CA, Universidad Nacional Pedro Ruiz Gallo, Lambayeque, Perú
[3] Grupo de investigación Biorrefinería, Facultad de Ingeniería Química y Textil, Universidad Nacional de Ingeniería, Perú
[4] Facultad Ingeniería Mecánica y Eléctrica, Universidad Tecnológica del Perú, Perú
[5] Grupo de Investigación Síntesis Química, Universidad Nacional Mayor de San Marcos, Perú
[6] Centro de Investigación de Ingeniería de Procesos de Tratamiento de Aguas, Universidad Nacional del Callao, Perú
* Corresponding author's e-mail: svasquezll@unprg.edu.pe

ABSTRACT

Tartrazine removal from tap water was evaluated using hydrodynamic cavitation with an orifice plate (2 mm thick, 9 orifices of 1 mm diameter) with a treatment time of 30 min, using the Taguchi L9 method with a signal-to-noise (S/N) criterion of larger-the-better. The factors evaluated were the inlet pressure to the orifice plate (2.5, 3.0, and 4.0 bar), the pH of the solution (3, 4, and 5), and the initial tartrazine concentration (5, 10, and 20 mg L^{-1}). pH was the only statistically significant factor ($p = 0.012$), contributing 96.12% to the total variation in the S/N ratio. The maximum color removal observed in the experimental design was 78.58% (3.0 bar, pH 3, and 10 mg L^{-1}). The optimal conditions determined by the Taguchi additive model (3.0 bar, pH 3, 5 mg L^{-1}) were validated through confirmatory testing, achieving a removal of 72.47% with a deviation of 1.34 % from the predicted S/N value (37.70 dB vs. 37.20 dB experimental), thus confirming its validity. The tartrazine degradation process followed pseudo-first-order kinetics with a rate constant $k_1 = 0.05634$ min^{-1} ($R^2 = 0.9081$). These results position hydrodynamic cavitation with an orifice plate as an efficient technology for treating water contaminated with azo dyes, with potential applications in drinking water treatment systems and municipal wastewater treatment plants.

Keywords: azo dyes, tartrazine removal, orifice plates, hydrodynamic cavitation, Taguchi analysis.

INTRODUCTION

Tartrazine is a recalcitrant anionic contaminant frequently detected in industrial process effluents and urban wastewater. Its chemical stability, intense color, and high water solubility make it difficult to remove using conventional treatment systems, raising considerable concerns about its environmental toxicity and the risks of human exposure [Arif, 2025]. Discharging these effluents into surface water bodies alters the pH, reduces oxygen levels, inhibits light penetration, and impairs photosynthetic activity. Furthermore, the persistent color in the effluents distorts the visual quality of the water, hindering its reuse [Srinivasan and Sadasivam, 2021].

Effluents containing azo dyes are conventionally treated using biological processes, adsorption, and coagulation-flocculation. However, these methods generate toxic byproducts and secondary pollution, demonstrating their inefficiency for the effective removal of azo dyes [Gawande et al., 2022]. Additionally, electrochemical oxidation and advanced sonochemical processes have high operating costs and energy requirements that limit their economic viability [Donoso et al., 2021]. Tartrazine removal from wastewater represents a significant environmental challenge, and the safety of water contaminated with tartrazine remains questionable. Therefore, the development of new, more efficient processes is needed to reduce environmental risks [Askarniya et al., 2022].

The hydrodynamic cavitation process is an advanced oxidation process in which the implosive collapse of microbubbles, generated when a fluid passes through a geometric constriction such as an orifice plate, produces extreme temperature and pressure conditions that dissociate water into •OH radicals capable of degrading recalcitrant organic compounds [Gawande et al., 2022]. During this process, the implosion of gas bubbles generates localized hot spots, leading to a sudden increase in both pressure and temperature within the treated medium. Additionally, the volatile organic contaminants present may infiltrate the formed cavities, and their subsequent high-energy implosion further enhances the efficiency of the oxidation process [Lebiocka, 2020]. Previous studies have demonstrated the effectiveness of hydrodynamic cavitation for tartrazine degradation [Askarniya et al., 2022; Gawande et al., 2022], most studies have addressed the isolated evaluation of variables or unifactorial designs, which restricts the understanding of the interactions among operational parameters and the assessment of process robustness to simultaneous disturbances in key factors such as the initial contaminant concentration, solution pH, and inlet pressure.

Despite the extensive literature on hydrodynamic cavitation for the degradation of synthetic dyes, the application of the Taguchi L9 orthogonal array combined with signal-to-noise ratio analysis and ANOVA-based percentage contribution for identifying significant operational factors in tartrazine degradation by hydrodynamic cavitation with an orifice plate has not been previously reported in the literature. Most published investigations have employed deionized or ultrapure water as the process matrix; however, tap water contains residual chlorine, dissolved carbonates, and bicarbonate species that function as hydroxyl radical scavengers, and its use as the process matrix provides experimental conditions more representative of actual drinking water treatment scenarios.

Therefore, this study evaluated the influence of inlet pressure (2.5, 3.0, and 4.0 bar), solution pH (3, 4, and 5), and initial tartrazine concentration (5, 10, and 20 mg L^{-1}) on color removal efficiency by orifice plate hydrodynamic cavitation using tap water as the aqueous matrix, employing the Taguchi L9 orthogonal array and signal-to-noise ratio analysis to identify the most influential operational factors and contribute to the development of efficient technologies for the reduction of synthetic azo dye contamination in drinking water systems.

MATERIALS AND METHODS

Materials

Tartrazine (purity ≥ 85%, Sigma-Aldrich, St. Louis, MO, USA) was used as the model azo dye contaminant in this study. Working solutions were prepared by dissolving the appropriate mass of tartrazine in tap water to achieve the initial concentrations established as control factors in the Taguchi L9 experimental design matrix (Table 1). Tap water was selected as the aqueous matrix to approximate realistic contamination scenarios in drinking water supply systems. The initial pH of tap water was 8.18 ± 0.05, determined at ambient temperature (25 ± 3 °C). Prior to each experimental run, the solution pH was adjusted to the levels specified in Table 1 by addition of HCl (1 mol L^{-1}) or NaOH (1 mol L^{-1}) as required, and monitored using a Hanna Instruments HI5221 pH meter, calibrated with standard buffer solutions at pH 4 and 7. All reagents employed for pH adjustment were of analytical grade purity.

Experimental setup

The experimental module comprised a 19 L stainless steel storage tank (component 8) fitted with a helical copper coil (component 9) supplied with recirculating cooling water to maintain the solution temperature at 30.9 ± 1.42 °C. The solution was circulated by a Pedrollo self-priming jet pump (0.75 kW, component 7) through a 1-inch nominal diameter stainless steel pipeline. Inlet pressure was regulated via the bypass line valve

Table 1. Controllable factors and their levels for the L9 orthogonal array

Factors	Description of factors	Levels		
		1	2	3
A	Inlet pressure (bar)	2.5	3.0	4.0
B	Solution pH	3	4	5
C	Initial concentration (mg L^{-1})	5	10	20

(component 1), which diverts a controlled fraction of the total flow back to the storage tank; the resulting line pressure and volumetric flow rate were monitored by pressure gauges (component 3) and a rotameter (component 6), respectively, both installed on the main line. Solution temperature at the inlet and outlet sections of the cavitation device was recorded using thermometers (component 2). The cavitation device consisted of a stainless-steel orifice plate (component 4) of 2 mm thickness with 9 circular orifices of 1 mm diameter arranged in a square configuration [Bocanegra et al., 2024], flanged within the main pipeline (component 5). The storage tank was further equipped with two stainless steel threaded nipples serving as a sampling port (component 10) for periodic aliquot withdrawal and a drain outlet (component 11) for solution discharge and equipment cleaning between experimental runs. A volume of 10 L of tartrazine solution was continuously recirculated through the system for a treatment time of 30 min per experimental run. The experimental module with orifice plate is shown in Figure 1.

The flow velocity in the cavitation device, the flow area, and the cavitation number are calculated using Equations 1, 2, and 3:

$$v = Q/A \tag{1}$$

where: Q is flow rate through hydrodynamic cavitation device ($m^3\ s^{-1}$), A is flow area (m^2), and v is velocity in the orifice plate ($m\ s^{-1}$).

$$A = \frac{n\pi d^2}{4} \tag{2}$$

where: n is number of orifices in the plate, and d is orifice diameter (m).

$$C_V = \frac{P_2 - P_v}{\frac{1}{2}\rho v^2} \tag{3}$$

where: P_2 is pressure at the outlet of the cavitation device (Pa), P_v is water vapor pressure (Pa), and ρ is density of fluid (1 000 kg m^{-3}).

Analytical methods

A stock solution of 20 mg L^{-1} tartrazine in tap water was prepared and used to obtain calibration standards by serial dilution at concentrations of 2, 5, 10, 15, and 20 mg L^{-1}. Absorbance of each standard was measured at the wavelength of maximum absorbance λ_{max} = 426 nm [Vaiano et al., 2016] using a Thermo Scientific Genesys 30 visible spectrophotometer. Linear regression of the absorbance-concentration data yielded the calibration equation, Equation 4, with a coefficient of determination $R^2 = 0.999$.

$$A = 0.0443 \times C + 0.0012 \tag{4}$$

where: A is absorbance and C is concentration in mg L^{-1}.

Samples collected at the end of the 30 min treatment period were analyzed at the same wavelength using the spectrophotometer previously programmed with the calibration equation.

Color removal efficiency was calculated for each replicate according to Equation 5, and results for each experimental run are reported as mean ± standard deviation of the three replicates.

$$\%\ color\ removal\ efficiency = \frac{C_0 - C_t}{C_0} \times 100 \tag{5}$$

where: C_0 and C_t are the initial and residual concentrations at the sampling time (mg L^{-1}), respectively.

Taguchi L9 experimental design

The operating conditions of the hydrodynamic cavitation process were optimized using the Taguchi method with an L9 (3^3) orthogonal array, enabling the evaluation of three factors at three levels. Inlet pressure levels of 2.5, 3.0, and 4.0 bar were selected to ensure fully developed cavitating flow ($C_V < 1$) across the entire evaluated range; solution pH levels of 3, 4, and 5 were

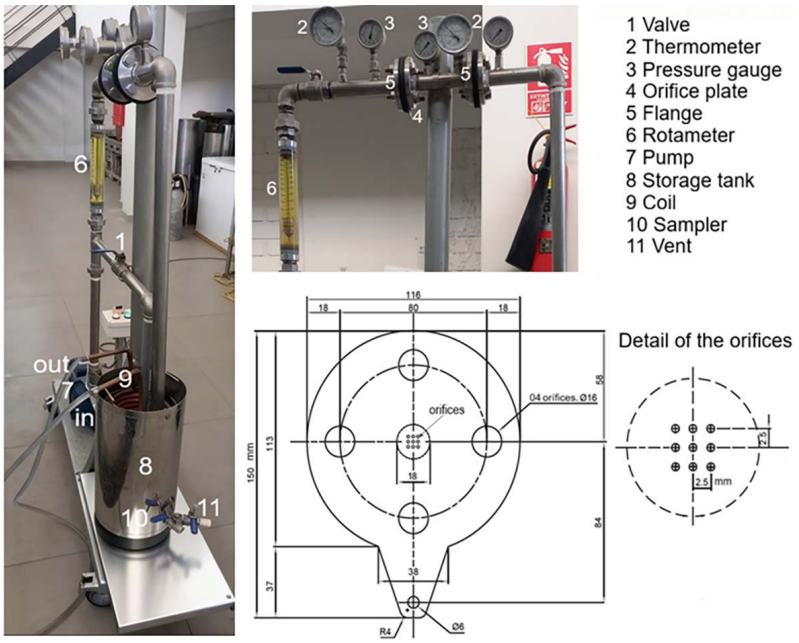

Figure 1. Experimental module with orifice plate

chosen to cover the acidic pH range in which hydroxyl radical oxidative efficiency is maximized for anionic dye molecules; and initial tartrazine concentrations of 5, 10, and 20 mg L^{-1} were selected to reflect realistic contamination levels in drinking water systems [Das et al., 2021; Gawande et al., 2022]. The control factors evaluated and their corresponding levels are presented in Table 1. The larger-is-better signal-to-noise (S/N) ratio criterion was applied as the performance metric and calculated according to Equation 6:

$$\frac{S}{N} = -10log\left[\frac{1}{n}\sum_{i=1}^{n}\frac{1}{y_i^2}\right] \quad (6)$$

where: S refer to the signal (mean) and N to the refer noise (standard deviation) of the input parameters, y is the output response, n is the number of replicates and i is the number of runs.

Each experimental combination was performed in triplicate, resulting in a total of 27 experimental runs. The order of the experiments was randomized to minimize the effect of uncontrolled sources of variation on the response. S/N ratio analysis, analysis of variance (ANOVA), and percentage contribution of each factor were performed using R version 4.4.0 within the RStudio integrated development environment version 2024.04.1. The percentage contribution of each factor was calculated according to Equation 7:

$$\rho_j = \frac{SS_j}{SS_T} \times 100 \quad (7)$$

where: ρ_j is the percentage contribution of factor j (%), SS_j is the sum of squares of factor j, and SS_T is the total sum of squares.

Optimal operating conditions were identified from the main effects plot of mean S/N ratios by selecting, for each factor independently, the level corresponding to the highest mean S/N ratio. Since this optimal combination was not included among the nine experimental runs of the L9 array, a confirmatory experiment was conducted under the identified optimal conditions.

Confirmation experiment

A confirmatory experiment was performed in triplicate under the optimal operating conditions identified from the main effects analysis of S/N ratios (3.0 bar, pH 3, 5 mg L^{-1}) to validate the predictive capacity of the Taguchi L9 orthogonal array design. The experimental S/N ratio was calculated from the triplicate color removal efficiency values obtained under optimal conditions according to the larger-is-better criterion, Equation 6. The predicted S/N ratio was estimated using the Taguchi additive model according to Equation 8:

$$\eta = \eta_m + \sum_{i=1}^{k}\left(\eta_{i,opt} - \eta_m\right) \quad (8)$$

where: η is the predicted S/N ratio (dB), η_m is the overall mean S/N ratio across all experimental runs (dB), $\eta_{i,opt}$ is the mean S/N ratio at the optimal level of factor i (dB), and k is the number of control factors ($k = 3$).

Validation was carried out by comparing the experimental S/N value obtained with the value predicted by the additive model according to Equation 9:

$$\Delta\eta = \left|\frac{\eta_{exp} - \eta}{\eta_{exp}}\right| \times 100 \quad (9)$$

where: $\Delta\eta$ is the percentage deviation (%), η_{exp} is the experimentally obtained S/N ratio (dB) under optimal conditions, and η is the predicted S/N ratio (dB) from the Taguchi additive model.

Kinetic analysis

The degradation kinetics of tartrazine were evaluated under the confirmed optimal operating conditions (3.0 bar, pH 3, and 5 mg L^{-1}) determined by the Taguchi method. Samples were collected at time intervals of 0, 4, 10, 15, 20, 25, and 30 min. The residual tartrazine concentration at each sampling time was determined directly from absorbance measurements at λ_{max} = 426 nm using the Thermo Scientific Genesys 30 visible spectrophotometer, previously programmed with the calibration equation, Equation 4. The pseudo-first-order kinetic model was fitted to the experimental concentration data by linearizing Equation 10:

$$\ln\left(\frac{C_0}{C_t}\right) = kt \quad (10)$$

where: C_0 is initial concentration of tartrazine (mg L^{-1}), C_t is remaining concentration of tartrazine (mg L^{-1}), k is first-order degradation rate constant (min^{-1}), and t is treatment time (min).

The goodness of fit was assessed using the coefficient of determination (R^2), the adjusted coefficient of determination (R^2_{adj}), and the root mean square error (RMSE). The statistical significance of the model was evaluated by the F-test p-value at a significance level of $\alpha = 0.05$. Normality of residuals was verified using the Shapiro-Wilk test, and homoscedasticity of residuals was assessed using the Breusch-Pagan test ($\alpha = 0.05$). All statistical analyses were performed using R version 4.4.0.

RESULTS AND DISCUSSION

Distribution of S/N ratios by Taguchi experiment

The distribution of S/N ratios across the experimental runs is shown in Figure 2, where the overall mean S/N ratio of 28.09 dB is indicated by the reference line. The experimental run conducted at 3.0 bar, pH 3, and 10 mg L^{-1} exhibited the highest S/N ratio de 37.09 dB, representing the best-performing condition within the L9 array, while the run at 2.5 bar, pH 4, and 10 mg L^{-1} yielded the lowest S/N ratio of 21.89 dB.

Effect of inlet pressure on hydrodynamic parameters and cavitation number

Table 2 presents the geometric and hydrodynamic parameters of the orifice plate at the three inlet pressures evaluated.

The cavitation number (C_V) decreased progressively from 0.75 to 0.47 as inlet pressure increased from 2.5 to 4.0 bar, accompanied by a corresponding increase in orifice velocity from 16.03 to 20.28 m s^{-1} and volumetric flow rate from 6.8 to 8.6 L min^{-1}, while downstream pressure remained constant at 101 325 Pa. Since the cavitation number is governed exclusively by inlet pressure and orifice geometry, the C_V values reported are independent of solution pH and initial tartrazine concentration, remaining constant across all experimental runs conducted at each pressure level.

Effective cavitation performance in orifice plate systems is generally observed within a cavitation number range of 0.1 to 1.0, wherein lower cavitation numbers increase cavitation intensity [Yeneneh et al., 2024]. All three evaluated conditions yielded $C_V < 1$, confirming the establishment of cavitating flow regimes across the entire experimental pressure range. In hydrodynamic cavitation systems, an increase in inlet pressure beyond an optimum value, the resulting formation of cavity clouds reduces the cavitational intensity, which negatively affects process performance [Thanekar et al., 2021]. Furthermore, the cavitation number, which characterizes the liquid's tendency to cavitate under specific conditions, does not always correlate with the final efficiency of the process; its performance is also influenced by other factors, such as the physicochemical properties of fluid and geometric parameters of the cavitation device [Rajoriya et al., 2017].

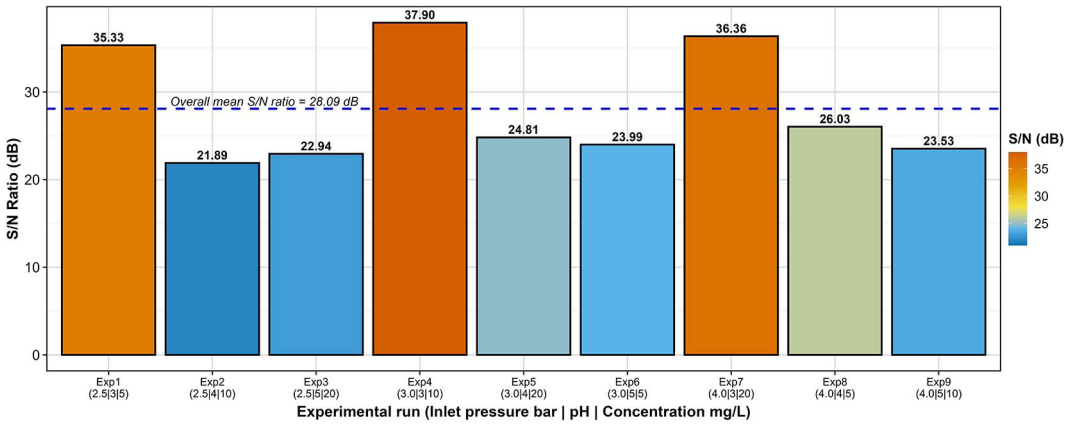

Figure 2. Distribution of S/N ratio by Taguchi experiment

In this regard, at C_V = 0.75 (2.5 bar), fully developed cavitating flow was established; however, the relatively elevated cavitation number indicates moderate cavitation intensity, yielding a color removal efficiency of 58.41%. The cavitation number alone is insufficient to capture the full complexity of the cavitation process and inadequate to precisely determine the specific conditions for cavitation inception, given its considerable dependence on multiple physical characteristics of the system [Yeneneh et al., 2024]. This observation further supports the integrated analysis of cavitation number and experimental color removal efficiency adopted in the present study to characterize the hydrodynamic performance of the orifice plate configuration. At C_V = 0.47 (4.0 bar), despite the further reduction in cavitation number, color removal efficiency decreased to 65.89%, confirming that process performance is not a monotonically increasing function of cavitation intensity.

The optimal cavitation number of approximately C_V = 0.55 identified in the present study at 3.0 bar is consistent with the range of effective cavitation performance reported for multi-orifice plate configurations, wherein optimized multi-orifice plate designs with nine orifices of 4 mm plate thickness have demonstrated minimum cavitation numbers of approximately 0.44, with maximum turbulence intensity, and vapor fraction corresponding to peak cavitation performance [Roy et al., 2025]. Among low-pressure non-rotary cavitation devices, the intensification of hydrodynamic cavitation has been shown to be strongly dependent on treatment parameters, and a critical analysis of reactor designs indicates that operating conditions must be carefully optimized for each specific device geometry to maximize cavitational yield and process efficiency [Das et al., 2021].

Taguchi L9 design matrix and experimental responses

Table 3 presents the nine experimental combinations, the color removal efficiency values obtained, and the S/N ratio calculated with the larger-is-better criterion.

Analysis of the experimental matrix and the S/N ratio shows that the optimal conditions correspond to the experiment with 3.0 bar, pH 3, and 10 mg L^{-1}. Under these conditions, the highest removal efficiency (78.58 ± 1.05%) and the highest S/N value (37.90) are achieved simultaneously. This result indicates not only superior performance but also greater robustness and stability

Table 2. Geometric and hydrodynamic parameters of orifice plate

Factor A, Pa	Solution temperature after 30 min, °C	Water vapor pressure, Pa	Flow rate, L min^{-1}	Flow area, m^2	Velocity, m s^{-1}	Downstream pressure, Pa	C_V
250 000	29.6 ± 0.82	4 150.42	6.8	7.0686e-6	16.03	101 325	0.75
300 000	30.6 ± 0.45	4 395.38	7.9		18.63	101 325	0.55
400 000	32.4 ± 0.13	4 868.08	8.6		20.28	101 325	0.47

Note: C_V is Cavitation Number, and Factor A is inlet pressure (Pa).

Table 3. Experimental design matrix and responses

Run	Factors			Absorbance			Concentration, C_t, mg L^{-1}			Color removal efficiency (%)			Mean color removal efficiency (%)	S/N ratio
	A	B	C	R1	R2	R3	R1	R2	R3	R1	R2	R3		
1	2.5	3	5	0.093	0.094	0.093	2.07	2.09	2.07	58.56	58.10	58.56	58.41 ± 0.27	35.33
2	2.5	4	10	0.388	0.389	0.39	8.73	8.75	8.78	12.69	12.46	12.16	12.44 ± 0.27	21.89
3	2.5	5	20	0.766	0.765	0.758	17.26	17.24	17.08	13.72	13.79	14.61	14.04 ± 0.49	22.94
4	3.0	3	10	0.101	0.096	0.092	2.25	2.13	2.04	77.47	78.68	79.58	78.58 ± 1.05	37.90
5	3.0	4	20	0.731	0.74	0.727	16.47	16.68	16.38	17.63	16.61	18.08	17.44 ± 0.75	24.81
6	3.0	5	5	0.187	0.188	0.188	4.20	4.22	4.21	15.97	15.67	15.87	15.84 ± 0.15	23.99
7	4.0	3	20	0.330	0.303	0.277	7.43	6.81	6.23	62.85	65.94	68.87	65.89 ± 3.01	36.36
8	4.0	4	5	0.177	0.177	0.181	3.96	3.98	4.05	20.78	20.48	18.98	20.08 ± 0.96	26.03
9	4.0	5	10	0.375	0.379	0.379	8.45	8.53	8.52	15.55	14.72	14.79	15.02 ± 0.46	23.53

Note: R means Replicate, C_t is Concentration at treatment time measured at 426 nm.

of the process against experimental disturbances. Within the framework of the Taguchi design, a high S/N value means maximizing the desired target variable with minimal variability. This suggests more reproducible operating conditions that are less sensitive to uncontrolled factors.

Effect of factors on the signal-to-noise ratio

The S/N ratio determined that solution pH is the dominant factor governing decolorization performance (Delta = 13.05; Rank 1), followed by the inlet pressure (Delta = 2.18; Rank 2) and the initial concentration of the dye (Delta = 0.68; Rank 3), as shown in Table 4. Furthermore, application of the larger-is-better Taguchi criterion to the three analyzed factors establishes as optimal operating conditions an inlet pressure of 3.0 bar, a solution pH of 3.0 and an initial tartrazine concentration of 5 mg L^{-1}, with the highest S/N ratio values of 28.90, 36.53 and 28.45 dB, respectively, as shown in Figure 3.

Effect of inlet pressure

As depicted in Figure 3a, the mean S/N ratio increased from 26.72 dB at 2.5 bar to 28.90 dB at 3.0 bar, then decreased to 28.64 dB at 4.0 bar, establishing 3.0 bar as the optimal inlet pressure level within the evaluated range. This behavior is consistent with the hydrodynamic mechanisms governing orifice plate cavitation systems. As inlet pressure increases from 2.5 to 3.0 bar, the fluid velocity through the orifice increases from 16.03 to 18.63 m s^{-1}. High-velocity flow through the orifice plate induces a low-pressure environment downstream of the restriction; when the local pressure drops below the vapor pressure of the fluid, cavitation is initiated, and flow separation occurs immediately after the orifice plate, a hydrodynamic behavior governed by the Bernoulli obstruction flow principle. A higher upstream pressure produces a lower cavitation number, forming a greater number of cavitation bubbles and leading to more intense cavitation [Chanphavong et al., 2025].

The collapse pressure and collapse temperature of the cavitation bubble increase with rising upstream inlet pressure; the associated intensification of the pressure gradient and turbulence enhances bubble collapse intensity, accelerating the dissociation of water molecules confined within the cavitation cavities and augmenting •OH radical production [Zhang et al., 2021; Roy et al., 2025]. Among the reactive oxygen species generated during bubble collapse, hydroxyl radicals (•OH) constitute the predominant fraction due to their high redox potential and non-selective reactivity toward organic pollutants; additional species produced include hydrogen peroxide, hydroperoxyl radicals (OH_2•), and atomic oxygen. Furthermore, excessive •OH generation may promote their accumulation within the boundary layer adjacent to the gas-liquid interface, limiting their availability for bulk-phase contaminant degradation [Sikora et al., 2026]. Moreover, the relationship between upstream pressure and •OH radical production follows a linear trend, whereby increasing inlet pressure directly enhances the generation of reactive species driving oxidative degradation; however, the relationship between hydraulic power and process efficiency is

Table 4. Response table of the S/N ratios for tartrazine color removal (larger-is-better)

Factors	Response (average) value			Delta	Rank
	1	2	3		
Inlet pressure (bar)	26.72	28.90	28.64	2.18	2
Solution pH	36.53	24.25	23.48	13.05	1
Initial concentration (mg L^{-1})	28.45	27.77	28.04	0.68	3

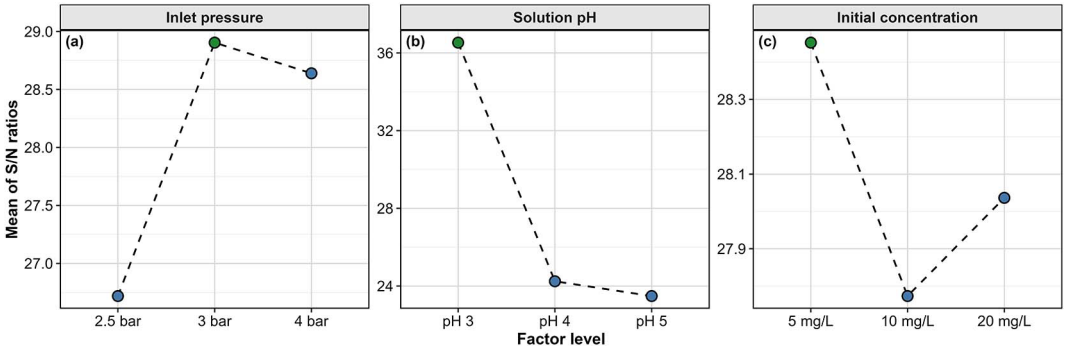

Figure 3. Main effects of: (a) inlet pressure, (b) solution pH, and (c) initial concentration

non-linear, as the energy dissipated through turbulence and associated losses increases disproportionately at higher pressures, reducing overall energy efficiency and underscoring the importance of identifying an optimal operating pressure that balances cavitation intensity with energy sustainability [Xiao et al., 2025].

The increase in inlet pressure promotes the formation of a greater number of cavities, intensifying the frequency of cavitation collapse and, consequently, the generation of •OH radicals available for dye degradation [Innocenzi et al., 2018]. The extreme local conditions generated during cavitation bubble collapse, including elevated temperatures, high pressures, shock waves, and high-velocity microjets, act in combination to intensify the degradation and transformation of organic compounds in water treatment applications [Ranade, 2022], collectively contributing to the oxidative degradation of the tartrazine chromophore under the cavitation conditions established in the present system. However, beyond an optimal threshold, the process efficiency decreases due to supercavitation [Mancuso et al., 2020]. Although elevated inlet pressure intensifies cavitation activity, pressures exceeding the optimal threshold promote the onset of supercavitation or choked cavitation conditions characterized by the formation of a saturated cavitation zone and the development of cavity cloud structures that impede the effective individual collapse of bubbles, thereby attenuating the net generation of hydroxyl radicals available for contaminant degradation [Ahmed et al., 2025].

At pressures above the optimum value, blocked cavitation conditions occur, compromising process efficiency; specifically, the excessive density of cavities generated leads to their coalescence into vapor bubbles that do not collapse and, therefore, do not interact with the dye molecules [Innocenzi et al., 2020]. Moreover, operating beyond the optimal pressure threshold yields no proportional improvement in color removal efficiency and results in increased energy consumption, limiting the economic feasibility and operational sustainability of the process at larger scales [Padoley et al., 2012]. In pilot hydrodynamic cavitation reactors with orifice plates, 4.0 bar has been identified as the pressure that maximizes color removal in industrial dyes [Zampeta et al., 2021], while in systems with a Venturi reactor, the maximum decolorization of tartrazine reached 16.36% operating in the 4.0 to 6.0 bar range [Askarniya et al., 2022]. The color removal efficiencies of 58.41%, 78.58%, and 65.89% observed at 2.5, 3.0, and 4.0 bar, respectively, as shown in Table 3, are consistent with this mechanistic interpretation, wherein the optimal balance between cavitation bubble density and individual collapse intensity is achieved at 3.0 bar under the evaluated experimental conditions.

The intensification of hydrodynamic cavitation is strongly dependent on treatment parameters, and operating conditions must be carefully selected to avoid supercavitation regimes that reduce cavitational yield [Das et al., 2021]. For tartrazine degradation by hydrodynamic cavitation, color removal efficiency increased progressively with inlet pressure up to an optimal value, beyond which a decrease in efficiency was observed due to the onset of choked cavitation, wherein the formation of a vapor cloud reduced the collapse pressure and the intensity of individual cavitational collapse events [Gawande et al., 2022]. In hydrodynamic cavitation systems for azo dye degradation, increasing pressure drop augments the number density of cavities; however, the coexistence of a greater number of cavities increases the effective compressibility of the medium, leading to a reduction in individual cavity collapse intensity, a lower generation of hydroxyl radicals, and consequently a reduced pollutant degradation rate [Merdoud et al., 2024]. These findings indicate that a cavitation number of 0.55 represents the optimal hydrodynamic condition for tartrazine decolorization in the current orifice plate configuration, beyond which further reductions in C_V are counterproductive to process efficiency.

The non-monotonic relationship between cavitation number and color removal efficiency identified in the present study is consistent with results reported for orifice plate hydrodynamic cavitation systems applied to the degradation of sulfonated azo dyes under acidic conditions, wherein an optimal inlet pressure was identified beyond which further increases yielded diminishing degradation returns [Rajoriya et al., 2017; Innocenzi et al., 2020]. In orifice plate hydrodynamic cavitation systems, inlet pressure determines the throat velocity and, consequently, the cavitation number; lower cavitation numbers result in a greater quantum of cavitation, whereas high cavitation intensity intensifies the dissociation of water molecules within the cavities and augments •OH radical production, underscoring the existence of an optimal operating pressure beyond which cavitation efficiency declines [Roy et al., 2025]. In the context of orifice plate hydrodynamic cavitation systems, inlet pressure values exceeding the optimal threshold promote the onset of supercavitation or choked cavitation conditions, characterized by the formation of a saturated cavitation zone and cavity cloud structures that impede effective individual bubble collapse and reduce overall process performance [Ahmed et al., 2025].

Effect of solution pH

As depicted in Figure 3b, the mean S/N ratio decreased from 36.53 to 23.48 dB at pH 3 to 23.48 at pH 5, establishing pH 3 as the optimal level within the evaluate range. This trend is consistent with findings reported for hydrodynamic cavitation (HC) systems applied to azo dyes removal, where decreasing pH progressively increases degradation performance, reaching decolorization efficiencies exceeding 70% under very acidic conditions, since the acidic medium suppresses •OH radical recombination and induces the transition of the dye molecules from their ionic to molecular form, reducing their hydrophilicity and their availability to interact with the undegraded species [Innocenzi et al., 2018]. The ionic form of the contaminant preferentially partitions into the bulk aqueous phase, reducing its exposure to the hydroxyl radicals generated at the cavitation bubble interface during collapse, whereas the molecular form exhibits a thermodynamic affinity for the gas-liquid interfacial region, where it undergoes preferential oxidative degradation by the locally concentrated •OH radicals [De-Nasri et al., 2022].

The generation of •OH radicals is further optimized under acidic pH by suppressing their recombination and intensifying the system's oxidizing potential [Rajoriya et al., 2017]. For anionic sulfonated azo dyes such as tartrazine, acidic conditions simultaneously enhance •OH availability and promote interfacial localization of the dye molecule, producing a dual mechanistic effect that substantially amplifies color removal efficiency. For anionic dyes, degradation efficiencies exceeding 75% have been reported after 180 minutes of treatment at pH 3, confirming that acidic conditions favor the performance of HC systems [Dhanke and Wagh, 2020]. The comparative analysis of pH effects across multiple HC studies consistently identifies the acidic pH range as the dominant operational parameter governing dye degradation efficiency, regardless of dye structure or cavitation device geometry. For tartrazine specifically, maximum degradation by HC alone was achieved at pH 2, with degradation efficiency decreasing progressively as pH increased toward neutral and alkaline conditions, attributable to the transition of the dye molecule from its molecular to its fully ionized form [Gawande et al., 2022].

Similarly, acidic conditions at pH 2 were identified as optimal for the degradation of methyl orange by orifice plate hydrodynamic cavitation,

with color removal efficiency at pH 2 exceeding that at pH 4 and 6 by more than 80% [Bagal et al., 2024]. For Direct Red 89, the highest removal efficiency of 75.4% was achieved at pH 3, whereas at pH 8 the removal efficiency decreased to 18.4%, demonstrating that decreasing pH from alkaline to acidic conditions substantially enhances the extent of dye degradation [Khajeh et al., 2022]. For Allura Red, maximum degradation of 76.48% by HC alone was obtained at 5 bar and pH 3 over 90 min, further corroborating the critical role of acidic pH in maximizing •OH-mediated color removal efficiency [Gawande et al., 2025]. These findings collectively confirm the dominance of solution pH observed in the present study, with a percentage contribution of 96.12% to the S/N ratio variance. The beneficial effect of acidic conditions is particularly pronounced at elevated inlet pressures, a behavior attributable to the synergistic interaction between cavitation intensity and radical chemistry: increased inlet pressure augments cavitation activity and the associated generation of •OH radicals, while the elevated concentration of H^+ ions under acidic conditions suppresses radical recombination, collectively enhancing the net oxidative capacity of the system [Innocenzi et al., 2022].

Effect of initial concentration

As depicted in Figure 3c, the mean S/N ratio reached its maximum value at an initial tartrazine concentration of 5 mg L^{-1} (28.45 dB), decreased at 10 mg L^{-1} (27.77 dB), and partially recovered at 20 mg L^{-1} (28.04 dB). The variation in S/N ratio across the three concentration levels, with a delta of 0.68 dB (Table 4) and a percentage contribution of 0.21% to the total variances (Table 5), indicates that initial tartrazine concentration exerted the least pronounced influence on color removal efficiency among the three factors evaluated, consistent with the low oxidative demand imposed by the dilute concentration range investigated relative to the •OH generation capacity of the system under the evaluated operating conditions. An increase in initial dye concentration imposes a proportionally greater demand on hydroxyl radical consumption; under constant operating conditions, the •OH radicals generated during cavitation bubble collapse, despite their finite availability, constitute the limiting reagent of the degradation reaction, and their insufficient supply relative to the increasing contaminant loading results in a reduction of the overall degradation yield [Innocenzi et al., 2020].

For tartrazine in hydrodynamic cavitation systems, increasing initial concentration determines a progressive decrease in degradation yield, as the molecular density of the dye in the aqueous phase does not correspond to a proportional enhancement in cavitational intensity under constant operating conditions [Gawande et al., 2022]. Furthermore, elevated contaminant loading attenuates the effective intensity of cavitational collapse and compromises mass transfer at the bubble–liquid interface, restricting contact between oxidative species and the target contaminant [Kentheswaran et al., 2022, 2023]. The partial recovery of the S/N ratio at 20 mg L^{-1} relative to 10 mg L^{-1} may be attributable to the increased probability of •OH contaminant encounters at higher molecular densities in the bulk aqueous phase, partially compensating for the reduced degradation yield per molecule; the differences between concentration levels remain within the experimental variability range and are not statistically significant, as evidenced by the low percentage contribution of this factor in the Taguchi ANOVA (0.21%), and the absence of statistical significance in the analysis of variance ($p = 0.842$), as shown Table 5.

The inverse relationship between initial concentration and degradation efficiency in hydrodynamic cavitation systems has been consistently reported for azo dyes across a range of concentrations and device configurations. For Allura Red, a structurally analogous anionic azo dye, degradation efficiency decreased progressively with increasing initial concentration under constant inlet pressure and pH conditions, confirming that the •OH generation capacity of the cavitation system constitutes the primary limiting factor at higher solute loadings [Gawande et al., 2025]. For methyl orange degradation by Venturi-based hydrodynamic cavitation, color removal efficiency decreased substantially with increasing initial concentration, with the highest degradation of 31.57% achieved at 5 mg L^{-1} after 60 min of treatment, whereas at concentrations of 10, 15, 20, and 25 mg L^{-1} the degradation efficiency declined progressively to 8.98%, 5.62%, 5.55%, and 4.50%, respectively, demonstrating that the •OH generation capacity of the cavitation device constitutes an effective upper limit beyond which increasing solute loading cannot be compensated by the available oxidative yield [Innocenzi et al., 2020].

As initial dye concentration increases, the total number of contaminant molecules in the aqueous phase augments while the •OH radical generation rate remains constant under fixed

hydrodynamic conditions, progressively reducing the degradation efficiency per unit mass of contaminant. The effective treatment of solutions at elevated dye concentrations would therefore require the incorporation of supplementary oxidant sources capable of augmenting •OH radical availability through synergistic advanced oxidation mechanisms [Innocenzi et al., 2022].

Effect of the aqueous matrix on factor responses

The trends observed across the three factors analyzed are further contextualized by the physicochemical characteristics of the aqueous matrix employed. Tap water contains minimal concentrations of organic pollutants and dissolved scavenger species, providing stable initial conditions for the experimental runs conducted [Sikora et al., 2026]. In real aqueous matrices containing elevated concentrations of radical scavengers such as carbonate or bicarbonate ions, pH adjustment as a pretreatment strategy has been recommended to mitigate their inhibitory effect on •OH availability; conversely, the presence of dissolved salts in such matrices may enhance the efficacy of hydrodynamic cavitation through salting effects that promote the localization of contaminant molecules at favorable positions within the collapsing cavitation bubbles [Das et al., 2021].

In the present study, these effects manifested in an attenuated manner, attributable to the use of tap water as the reaction matrix, a condition that constrains the presence of competing species for •OH radicals and accounts for the moderate color removal efficiencies observed across the evaluated factor levels without reaching statistical significance under the Taguchi L9 design employed for inlet pressure and initial concentration. In experimental studies on advanced oxidation processes applied to reactive azo dyes, complete color removal was achievable within 15 min in the absence of radical scavenger species; however, the rate of color removal was substantially attenuated with increasing concentrations of bicarbonate and carbonate ions, particularly under alkalinity conditions where carbonate ions predominated [Gultekin and Ince, 2004]. This finding underscores the relevance of matrix composition as a determinant of process performance in hydrodynamic cavitation systems and supports the use of tap water as a representative matrix for drinking water treatment applications.

Analysis of variance and percentage contribution

The analysis of variance (ANOVA) of the signal-to-noise ratio for tartrazine color removal by hydrodynamic cavitation is presented in Table 5.

The pH of the solution was the only statistically significant factor ($F = 85.62$; $p = 0.012$) and explained 96.12% of the variability in decolorization efficiency, indicating its dominant influence on process dynamics. In hydrodynamic cavitation systems for dye decomposition, an acidic pH has been identified as the factor with the greatest influence on process efficiency [Das et al., 2021]. Accordingly, at pH 2.5, removal efficiencies of over 60% have been documented after 120 minutes of treatment with a single-slot Venturi device. This behavior is associated with increased pollutant transport into the cavitation collapse zones and the intensification of oxidative processes [Momin and Gogate, 2024].

Specifically for tartrazine, it has been documented that the initial pH significantly influences the decolorization efficiency in hydrodynamic cavitation reactors. The maximum degradation rate occurs under acidic conditions and decreases with increasing pH towards alkaline values [Gawande et al., 2022]. The inlet pressure ($p = 0.306$) and outlet concentration ($p = 0.842$) were not statistically significant, with proportions of 2.55% and 0.21%, respectively. This suggests that these factors do not have a statistically

Table 5. S/N ratio analysis of variance (ANOVA) for tartrazine color removal

Source	Df	Sum of squares	Mean square	F-value	p-value	% Contribution
Inlet pressure (bar)	2	8.533	4.266	2.27	0.306	2.55
Solution pH	2	321.662	160.831	85.62	0.012	96.12
Initial concentration (mg L^{-1})	2	0.703	0.351	0.19	0.842	0.21
Error	2	3.757	1.878			1.12
Total	8	334.654				100

Note: % contribution calculated using Equation 7.

significant influence on the signal-to-noise ratio (S/N) of the process within the investigated range. However, the physical effect of the inlet pressure on the decolorization efficiency is clearly evident in the main effect analysis (Delta = 2.18), which is consistent with the mechanisms of cavitation formation and cavitation collapse [Momin and Gogate, 2024].

The initial concentration, with the lowest delta value (0.68) among the investigated factors, shows only a minor influence on the variability of the system response. This result is consistent with radical scavenging mechanisms. This behavior is attributed to the attenuated influence of this factor within the analyzed concentration range in a drinking water matrix, where the low levels of dissolved organic matter and inorganic ions reduce radical scavenging processes and limit the generation of additional competing species that could otherwise enhance its effect on the process [Hübner et al., 2024; Lado Ribeiro et al., 2019]. The experimental error of 1.12% indicates that the three selected factors explain 98.88% of the total variability of the system, with a minimal contribution from uncontrolled sources. This confirms the robustness of the Taguchi L9 design, which was used to optimize tartrazine decolorization via hydrodynamic cavitation.

Optimal conditions and experimental validation

The confirmatory experiment was performed three times under the optimal conditions predicted by the Taguchi additive model (3.0 bar, pH 3, 5 mg L^{-1}). A tartrazine dye removal efficiency of 72.47% was obtained, with an experimental signal-to-noise ratio (S/N) of 37.20 dB, as shown Table 6. The predicted S/N was 37.70 dB, with a difference of 1.34% between the two values. This confirms the predictive power of the Taguchi L9 design and the validity of the additivity assumption between the factors within the investigated range. This agreement is consistent with the results of optimization studies that applied the Taguchi L9 design for dye removal in advanced oxidation processes. There, deviations between the predicted and experimental S/N values of less than 5% confirm the validity of the additivity assumption between the factors and the predictive reliability of the additive model [S & R, 2023].

The removal efficiency determined under the confirmed optimal conditions (72.47%) was comparable to that obtained in the highest-performing run of the L9 system, specifically run 4 (3.0 bar, pH 3, 10 mg L^{-1}), which achieved 78.58 ± 1.05% and a signal-to-noise ratio of 37.90 dB. The difference is due to the reduction of the initial concentration from 10 to 5 mg L^{-1}. This reduces the total amount of dye that can be degraded by the •OH radicals generated during cavitation collapse without significantly affecting the relative efficiency of the process. From an operational perspective, this result is significant because it demonstrates that the hydrodynamic cavitation system with an orifice plate maintains a removal efficiency of over 70% even in low-concentration solutions, a typical condition for drinking water contaminated with tartrazine. In hydrodynamic cavitation systems specifically designed for tartrazine, decolorization efficiencies exceeding 75% have been documented under acidic conditions and at inlet pressures of 3.0 to 6.0 bar [Gawande et al., 2022]. The value determined in this study falls within this performance range. Experimental validation confirms that the Taguchi L9 design represents a reliable methodological strategy for determining optimal conditions for azo dye removal in hydrodynamic cavitation systems with an orifice plate.

Tartrazine degradation kinetics

The visual evidence of the progressive decolorization of the tartrazine solution under the confirmed optimal operating conditions (3.0 bar, pH 3, 5 mg L^{-1}) is shown in Figure 4. The chromatic transition from the intense yellow characteristic of the dye in aqueous solution toward progressively more attenuated hues qualitatively

Table 6. Experimental validation of optimal conditions predicted by Taguchi additive model

Run	Absorbance	Concentration at 30 min	Color removal efficiency (%)	Mean color removal efficiency (%)	Experimental S/N ratio	Predicted S/N ratio	% Deviation
R1	0.058	1.32	73.6	72.47 ± 1.20	37.20	37.70	1.34
R2	0.060	1.37	72.6				
R3	0.063	1.44	71.2				

Note: Experimental and predicted S/N ratio, and % deviation was calculated using Equation 6, 8, and 9, respectively.

corroborates the pseudo-first-order (PFO) kinetic behavior instrumentally determined.

The graphical diagnostic analysis depicted in Figure 5: residuals vs fitted values (Figure 5a) and normal Q-Q plot (Figure 5b), corroborated the statistical assumption tests (Shapiro-Wilk W = 0.9564, p = 0.7875; Breusch-Pagan χ^2 = 0.2163, p = 0.6418), confirming that the pseudo-first-order kinetic model residuals satisfy the assumptions of normality and homoscedasticity.

The temporal variation of tartrazine concentration under the determined optimum conditions (3.0 bar, pH 3, 5 mg L^{-1}) was fitted to the pseudo-first-order kinetic model using the linearized representation $\ln(C_0/C_t) = k_1 * t$ without intercept, whose linear behavior is shown in Figure 6a, demonstrating that the degradation rate is proportional to the instantaneous concentration of the contaminant in the bulk solution. The determined pseudo-first-order rate constant was k_1 = 0.05634 min^{-1} (95% CI: 0.0384 – 0.0742 min^{-1}), with a coefficient of determination R^2 = 0.9081, R^2adj = 0.8928 and RMSE = 0.3224, statistically significant (p = 0.000251), indicating a satisfactory fit of the experimental data to the proposed model. The calculated half-life was t½ = 12.30 min, as shown in Figure 6b, which establishes that half of the initial concentration of tartrazine was degraded in the first 12.30 min of treatment under the action of the •OH radicals generated during cavitation collapse.

Scientific literature reports that the degradation of organic compounds by hydrodynamic cavitation is frequently described using a pseudo-first-order kinetic model, particularly in systems where the rate-limiting step is associated with the reaction with in situ generated free radicals [Rajoriya et al., 2017]. The kinetic constant k_1 = 0.05634 min^{-1} determined in this study is at the upper end of the range of values reported in the literature for the degradation of organic dyes by hydrodynamic cavitation with an orifice plate under acidic conditions, as shown in Table 7. These differences are attributable to variations in the geometry of the cavitation device, the inlet pressure, the aqueous matrix used, the specific molecular structure of the dye being treated, and the initial concentration of the dye [Askarniya et al., 2022; Gawande et al., 2022].

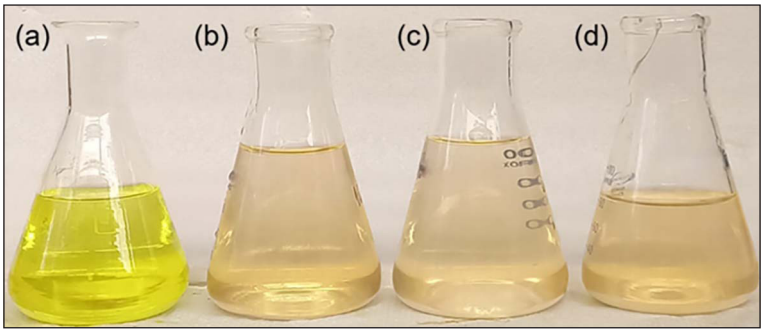

Figure 4. Progressive tartrazine decolorization under optimal conditions (3.0 bar, pH 3, 5 mg L-1): (a) 0 min (b) 10 min, (c) 20 min, and (d) 30 min

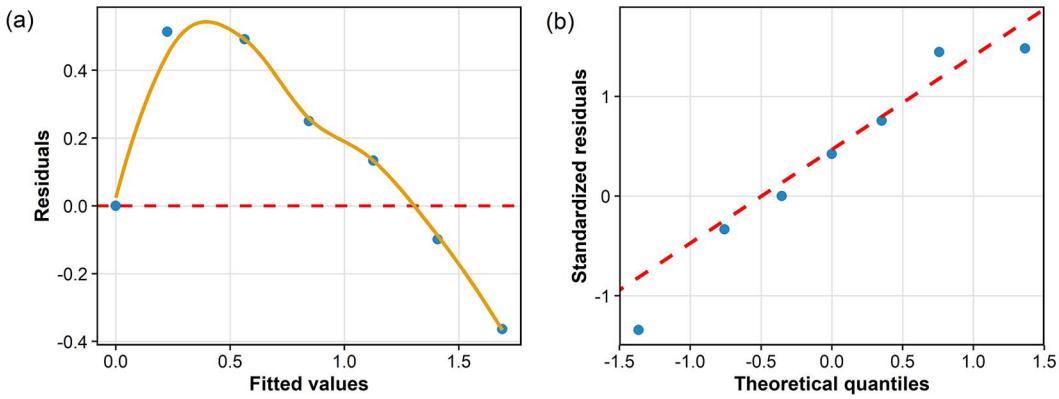

Figure 5. Diagnostic plots of the pseudo-first-order kinetics model: (a) residuals vs fitted values, and (b) normal Q-Q plot standardized residuals

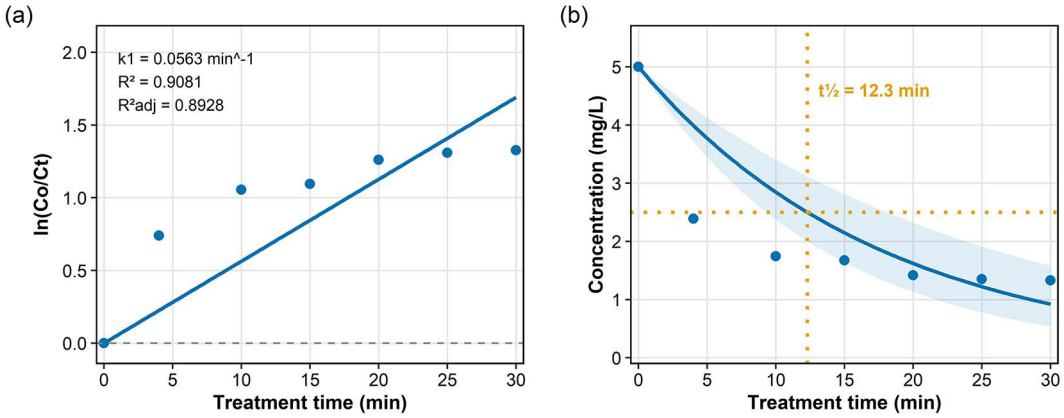

Figure 6. Analysis of tartrazine degradation: (a) kinetic model, and (b) degradation profile

Table 7. PFO order constants for the degradation of dyes by hydrodynamic cavitation

Dye	Device	Conditions	k_1 (min^{-1})	R^2	Study
Tartrazine	Orifice plate	3.0 bar, pH 3, 5 mg L^{-1}, 30 min	0.05634	0.9081	Present study
Reactive blue 13	Slit Venturi	4.0 bar, pH 2, 30 mg L^{-1}, 120 min	0.0052	____	[Rajoriya et al., 2017]
Methyl orange	Venturi reactor	2.0 bar, pH 2, 5 mg L^{-1}, 60 min	0.0089	> 0.99	[Innocenzi et al., 2018]
Tartrazine	Circular Venturi	5.0 bar, pH 2, 50 mg L^{-1}, 60 min	0.002	____	[Gawande et al., 2022]
Orange II sodium	Venturi and Orifice plate	3.0 bar, pH 2, 20 mg L^{-1}, 10 min	0.0808	0.9228	[Kakama et al., 2024]

The adequate predictive capacity of the pseudo-first order kinetic model, together with the determined k_1 and t½ parameters, corroborates that the optimal conditions established by the Taguchi L9 design not only maximize the overall color removal efficiency, but also intensify the chromophore degradation rate, providing mechanistic coherence and experimental consistency to the optimization process developed for tartrazine decolorization by hydrodynamic cavitation with orifice plate [Askarniya et al., 2022; Shokoohi et al., 2023].

CONCLUSIONS

The present study demonstrated that hydrodynamic cavitation employing an orifice plate constitutes an effective alternative for the removal of tartrazine from tap water. Using a Taguchi L9 design, solution pH was identified as the dominant operational factor (contribution = 96.12%, p = 0.012), whereas inlet pressure and initial concentration did not exhibit a statistically significant effect on process efficiency. The maximum color removal achieved was 78.58% at 3.0 bar, pH 3, and 10 mg L^{-1}. The optimal conditions predicted by the additive model (3.0 bar, pH 3, 5 mg L^{-1}) were experimentally validated, yielding a removal efficiency of 72.47% with a deviation of 1.34% from the predicted value, thereby confirming the robustness of the model. Kinetic analysis revealed pseudo-first-order behavior, with a rate constant k_1 = 0.05634 min^{-1} and a half-life of approximately 12.3 min. These findings position hydrodynamic cavitation with an orifice plate as an efficient advanced oxidation technology for the treatment of water contaminated with azo dyes, with potential applicability in drinking water systems and municipal treatment facilities. Furthermore, future investigations should consider the integration of computational fluid dynamics modelling to characterize the cavitation flow field within the orifice plate geometry, providing a deeper understanding of the hydrodynamic mechanisms governing bubble formation, collapse dynamics, and hydroxyl radical spatial distribution under the optimal operating conditions identified in the present study.

Acknowledgements

This work is supported by "Vicerrectorado de Investigación de la Universidad Nacional Pedro Ruiz Gallo".

REFERENCES

1. Ahmed, D., Aboulfotoh, A. M., Elsafty, Z. (2025). Harnessing hydrodynamic cavitation, alkaline treatments and advanced oxidation processes for enhancement of sludge disintegration. *Journal of Ecological Engineering*, *26*(10). https://doi.org/10.12911/22998993/207192
2. Arif, M. (2025). Adsorptive removal and photocatalytic degradation of tartrazine: A critical review. *Journal of Alloys and Compounds*, *1046*, 184820. https://doi.org/10.1016/j.jallcom.2025.184820
3. Askarniya, Z., Baradaran, S., Sonawane, S. H., Boczkaj, G. (2022). A comparative study on the decolorization of Tartrazine, Ponceau 4R, and Coomassie Brilliant Blue using persulfate and hydrogen peroxide based Advanced Oxidation Processes combined with Hydrodynamic Cavitation. *Chemical Engineering and Processing - Process Intensification*, *181*, 109160. https://doi.org/10.1016/j.cep.2022.109160
4. Bagal, M. V., Rajan, V., Shinde, S., Banerjee, B. V., Gole, V., Mohod, A. V. (2024). Degradation of azo dyes using hydrodynamic cavitation and external oxidants. *Advances in Environmental Technology*. https://doi.org/10.22104/aet.2024.6092.1679
5. Bocanegra, K. E. C., Llanos, S. A. V., Chuquizuta, J. C. M., Quispe, A. P. B., Purihuaman, M. S., Scheineder, S. H., Carreño-Farfan, C., Collana, J. T. M. (2024). Removal of color and polyphenols from sugarcane molasses ethanol vinasse by hydrodynamic cavitation. *Chemical Engineering Transactions*, *114*, 1117-1122. https://doi.org/10.3303/CET24114187
6. Chanphavong, L., Chanthaboune, V., Phonhalath, K. (2025). CFD Analysis of hydrodynamic cavitation through an orifice: Influence of different inlet pressures and number of orifice holes. *ASEAN Journal on Science and Technology for Development*, *42*(1). https://doi.org/10.61931/2224-9028.1603
7. Das, S., Bhat, A. P., Gogate, P. R. (2021). Degradation of dyes using hydrodynamic cavitation: Process overview and cost estimation. *Journal of Water Process Engineering*, *42*, 102126. https://doi.org/10.1016/j.jwpe.2021.102126
8. De-Nasri, S. J., Sarvothaman, V. P., Nagarajan, S., Manesiotis, P., Robertson, P. K. J., Ranade, V. V. (2022). Quantifying OH radical generation in hydrodynamic cavitation via coumarin dosimetry: Influence of operating parameters and cavitation devices. *Ultrasonics Sonochemistry*, *90*, 106207. https://doi.org/10.1016/j.ultsonch.2022.106207
9. Dhanke, P. B., Wagh, S. M. (2020). Intensification of the degradation of Acid RED-18 using hydrodynamic cavitation. *Emerging Contaminants*, *6*, 20–32. https://doi.org/10.1016/j.emcon.2019.12.001
10. Donoso, G., Dominguez, J. R., González, T., Correia, S., Cuerda-Correa, E. M. (2021). Electrochemical and sonochemical advanced oxidation processes applied to tartrazine removal. Influence of operational conditions and aqueous matrix. *Environmental Research*, *202*, 111517. https://doi.org/10.1016/j.envres.2021.111517
11. Gawande, G. D., Nahata, Y. D., Chavan, P. V. (2025). Allura Red dye degradation using hybrid advanced oxidation methods. *Chemical Papers*, *79*(3), 1879–1889. https://doi.org/10.1007/s11696-025-03895-y
12. Gawande, G. D., Pinjari, D. V., Chavan, P. V. (2022). Degradation of tartrazine using hydrodynamic cavitation-based hybrid techniques and Fenton chemistry. *Chemical Engineering & Technology*, *45*(6), 1148-1157. https://doi.org/10.1002/ceat.202100419
13. Gultekin, I., Ince, N. H. (2004). Degradation of reactive azo dyes by UV/H2O2: Impact of radical scavengers. *Journal of Environmental Science and Health, Part A*, *39*(4), 1069–1081. https://doi.org/10.1081/ESE-120028414
14. Hübner, U., Spahr, S., Lutze, H., Wieland, A., Rüting, S., Gernjak, W., Wenk, J. (2024). Advanced oxidation processes for water and wastewater treatment – Guidance for systematic future research. *Heliyon*, *10*(9), e30402. https://doi.org/10.1016/j.heliyon.2024.e30402
15. Innocenzi, V., Prisciandaro, M., Tortora, F., Vegliò, F. (2018). Optimization of hydrodynamic cavitation process of azo dye reduction in the presence of metal ions. *Journal of Environmental Chemical Engineering*, *6*(6), 6787–6796. https://doi.org/10.1016/j.jece.2018.10.046
16. Innocenzi, V., Prisciandaro, M., Vegliò, F. (2020). Study of the effect of operative conditions on the decolourization of azo dye solutions by using hydrodynamic cavitation at the lab scale. *The Canadian Journal of Chemical Engineering*, *98*(9), 1980–1988. https://doi.org/10.1002/cjce.23782
17. Innocenzi, V., Colangeli, A., Prisciandaro, M. (2022). Advanced oxidation processes for the removal of dyes from synthetic industrial wastewaters. *Desalination and Water Treatment*, *259*, 315–320. https://doi.org/10.5004/dwt.2022.28629
18. Kakama, N. K., Petrik, L. F., Ojumu, T. V. (2024). The optimization of hydrodynamic cavitation as an advanced oxidation option for the removal of persistent contaminants in wastewater. *Water, Air, & Soil Pollution*, *235*(3), 193. https://doi.org/10.1007/s11270-024-06924-w
19. Khajeh, M., Taheri, E., Amin, M. M., Fatehizadeh, A., Bedia, J. (2022). Combination of hydrodynamic cavitation with oxidants for efficient treatment of synthetic and real textile wastewater. *Journal of Water Process Engineering*, *49*, 103143. https://doi.org/10.1016/j.jwpe.2022.103143
20. Kentheswaran, K., Antier, W., Dietrich, N., Lalanne, B. (2023). Impact of surfactants on the rise of deformable bubbles and interfacial gas–liquid mass transfer. Journal of fluid mechanics. *Cambridge Core*, *970*. https://doi.org/10.1017/jfm.2023.592

21. Kentheswaran, K., Dietrich, N., Tanguy, S., Lalanne, B. (2022). Direct numerical simulation of gas-liquid mass transfer around a spherical contaminated bubble in the stagnant-cap regime. *International Journal of Heat and Mass Transfer*, *198*, 123325. https://doi.org/10.1016/j.ijheatmasstransfer.2022.123325
22. Lado Ribeiro, A. R., Moreira, N. F. F., Li Puma, G., Silva, A. M. T. (2019). Impact of water matrix on the removal of micropollutants by advanced oxidation technologies. *Chemical Engineering Journal*, *363*, 155–173. https://doi.org/10.1016/j.cej.2019.01.080
23. Lebiocka, M. (2020). Application of hydrodynamic cavitation to improve the biodegradability of municipal wastewater. *Journal of Ecological Engineering*, *21*(6), 155–160. https://doi.org/10.12911/22998993/123163
24. Mancuso, G., Langone, M., Andreottola, G. (2020). A critical review of the current technologies in wastewater treatment plants by using hydrodynamic cavitation process: Principles and applications. *Journal of Environmental Health Science and Engineering*, *18*(1), 311–333. https://doi.org/10.1007/s40201-020-00444-5
25. Merdoud, R., Aoudjit, F., Mouni, L., Ranade, V. V. (2024). Degradation of methyl orange using hydrodynamic Cavitation, H_2O_2, and photo-catalysis with TiO2-Coated glass Fibers: Key operating parameters and synergistic effects. *Ultrasonics Sonochemistry*, *103*, 106772. https://doi.org/10.1016/j.ultsonch.2024.106772
26. Momin, R. F., Gogate, P. R. (2024). Degradation of reactive violet 1 using innovative approach of hydrodynamic cavitation coupled with oxidants. *Chemical Engineering Science*, *298*, 120414. https://doi.org/10.1016/j.ces.2024.120414
27. Padoley, K. V., Saharan, V. K., Mudliar, S. N., Pandey, R. A., Pandit, A. B. (2012). Cavitationally induced biodegradability enhancement of a distillery wastewater. *Journal of Hazardous Materials*, *219–220*, 69–74. https://doi.org/10.1016/j.jhazmat.2012.03.054
28. Rajoriya, S., Bargole, S., Saharan, V. K. (2017). Degradation of reactive blue 13 using hydrodynamic cavitation: Effect of geometrical parameters and different oxidizing additives. *Ultrasonics Sonochemistry*, *37*, 192–202. https://doi.org/10.1016/j.ultsonch.2017.01.005
29. Ranade, V. V. (2022). Modeling of hydrodynamic cavitation reactors: Reflections on present status and path forward. *ACS Engineering Au*, *2*(6), 461–476. https://doi.org/10.1021/acsengineeringau.2c00025
30. Roy, S., Rudra, S., Muhandiram, D., Roshid, M. (2025). Numerical modelling and experimental validation of an orifice plate-based hydrodynamic cavitation process for improving the biomass pretreatment. *Biotechnology Reports*, *48*, e00925. https://doi.org/10.1016/j.btre.2025.e00925
31. S, M., R, S. (2023). Textile dye effluent treatment using advanced sono-electrocoagulation techniques: A Taguchi and particle swarm optimization modeling approach. *Energy Sources, Part A: Recovery, Utilization, and Environmental Effects*, *45*(2), 4501–4519. https://doi.org/10.1080/15567036.2023.2205356
32. Shokoohi, R., Rahmani, A., Asgari, G., Ashrafi, M., Ghahramani, E. (2023). Removal of algae using hydrodynamic cavitation, ozonation and oxygen peroxide: Taguchi optimization (case study: Raw water of sanandaj water treatment plant). *Process Safety and Environmental Protection*, *169*, 896–908. https://doi.org/10.1016/j.psep.2022.11.057
33. Sikora, P., Fialová, S., Pochylý, F., Maršálková, E. (2026). Theoretical framework and preliminary experimental evaluation of magnetically enhanced production of hydroxyl radicals in cavitating flows for wastewater treatment. *Journal of Ecological Engineering*, *27*(3). https://doi.org/10.12911/22998993/213631
34. Srinivasan, S., Sadasivam, S. K. (2021). Biodegradation of textile azo dyes by textile effluent non-adapted and adapted *Aeromonas hydrophila*. *Environmental Research*, *194*, 110643. https://doi.org/10.1016/j.envres.2020.110643
35. Thanekar, P., Gogate, P. R., Znak, Z., Sukhatskiy, Yu., Mnykh, R. (2021). Degradation of benzene present in wastewater using hydrodynamic cavitation in combination with air. *Ultrasonics Sonochemistry*, *70*, 105296. https://doi.org/10.1016/j.ultsonch.2020.105296
36. Vaiano, V., Iervolino, G., Sannino, D. (2016). Photocatalytic removal of tartrazine dye from aqueous samples on $LaFeO_3$/ZnO photocatalysts. *Chemical Engineering Transactions*, *52*, 847–852. https://doi.org/10.3303/CET1652142
37. Xiao, J., Dommke, M., Franke, M., Stelter, M., Braeutigam, P. (2025). Integrated characterization of hydrodynamic cavitation: Optical, chemical, and simulation correlations. *Chemical Engineering Science*, *306*, 121239. https://doi.org/10.1016/j.ces.2025.121239
38. Yeneneh, A. M., Balushi, K. A., Jafary, T., Marshudi, A. S. A. (2024). Hydrodynamic cavitation and advanced oxidation for enhanced degradation of persistent organic pollutants: A review. *Sustainability*, *16*(11). https://doi.org/10.3390/su16114601
39. Zhang, X., Zhu, X., Cao, Y., Zhang, K., Huang, Y., Yang, F., Ren, X. (2021). Analysis of the influencing factors of the hydroxyl radical yield in a hydrodynamic cavitation bubble of a chitosan solution based on a numerical simulation. *ACS Omega*, *6*(5), 3736–3744. https://doi.org/10.1021/acsomega.0c05335
40. Zampeta, C., Bertaki, K., Triantaphyllidou, I.-E., Frontistis, Z., Vayenas, D. V. (2021). Treatment of real industrial-grade dye solutions and printing ink wastewater using a novel pilot-scale hydrodynamic cavitation reactor. *Journal of Environmental Management*, *297*, 113301. https://doi.org/10.1016/j.jenvman.2021.113301